J. Fluid Mech. (1998), *vol.* 359, *pp.* 165–180. Printed in the United Kingdom

Instability of thermocapillary–buoyancy convection in shallow layers. Part 2. Suppression of hydrothermal waves

By S. BENZ[1], P. HINTZ[1], R. J. RILEY[2] AND G. P. NEITZEL[3]

[1] Physikalisches Institut, Universität Gießen, Germany

[2] Cabot Corporation, Research and Development, Pampa, TX 79066, USA.

[3] The George W. Woodruff School of Mechanical Engineering, Georgia Institute of Technology, Atlanta, GA 30332-0405, USA

(Received 5 October 1996 and in revised form 12 November 1997)

Hydrothermal-wave instabilities in thermocapillary convection are known to produce undesirable effects when they occur during the float-zone crystal-growth process, and perhaps in other situations. Suppression of the hydrothermal-wave instability produced in the model system of Part 1 (Riley & Neitzel 1998) is demonstrated through the sensing of free-surface temperature perturbations and the periodic addition of heat at the free surface along lines parallel to the crests of the hydrothermal waves.

1. Introduction

The onset of oscillatory thermocapillary convection during the float-zone crystal-growth process is thought to be responsible for the appearance of undesirable striations in material resulting from the process. This is shown convincingly in experiments reported by Gatos (1982), in which the heater current was oscillated during crystal growth from melt and dopant striations observed in the resulting crystal could be correlated with the imposed temporal oscillations. Analyses of the stability of thermocapillary convection in half-zone models of the float-zone process, such as those performed by Shen *et al.* (1990), Neitzel *et al.* (1991), Wanschura *et al.* (1995) and Levenstam & Amberg (1995), yield results which identify regions of either guaranteed stability (energy theory) or guaranteed instability (linear theory). In the case of an actual crystal-growth situation, such results (were they even available) may not be of practical utility, since the crystal grower has little latitude in setting operating conditions to, say, keep the Marangoni number within a region known to be free of instability. In such a situation, it may be worthwhile to explore the possibility of suppressing oscillatory thermocapillary convection, should it occur. This provides the motivation for the present work.

Riley & Neitzel (1998) (hereafter referred to as Part 1) have experimentally demonstrated the existence of the hydrothermal-wave instability predicted by Smith & Davis (1983) in thin layers of silicone oil for which buoyancy forces are quite small. This instability is characterized by the appearance of a single family of thermal waves which propagate obliquely across the layer at an angle which depends on the Prandtl number of the liquid. Smith (1986) has discussed the instability mechanism for this convective instability: for the high-Prandtl-number case appropriate to the oil used in the experiments of Part 1, there is an interaction between the temperature fluctuations

on the free surface and the bulk temperature which sustains the hydrothermal waves. Hence, interference with this mechanism through the modification of the free-surface temperature may provide a way to delay the onset of the undesirable oscillations. For the case of classical Rayleigh–Bénard convection, Tang & Bau (1993) have demonstrated theoretically the possibility of delaying the onset of convection significantly through local modification of the temperature of the bottom wall.

Additional motivation for undertaking an approach of this type is provided by the experiments of Liepmann, Brown & Nosenchuck (1982) and Liepmann & Nosenchuck (1982), who used periodic surface strip heating to suppress the growth of both artificially induced disturbances and naturally occurring Tollmien–Schlichting (T–S) waves in a laminar boundary layer on a flat plate. In the latter case, the appearance of T–S waves was delayed significantly. These experiments were performed in water and the periodic heating, through the reduction of viscosity, mimicked the action of periodic suction at the wall. The actuation of the heating was provided by the signal from an upstream wall-shear-stress sensor.

The present experiments utilize the ideas employed by Liepmann & Nosenchuck (1982), along with the theoretical basis provided by Smith (1986), to demonstrate that suppression of hydrothermal waves is possible in thin layers dominated by thermocapillarity. Sensing of free-surface temperature fluctuations is accomplished non-intrusively in real time using an infrared (IR) camera. Surface heating is delivered to the layer in the form of a thin sheet of infrared radiation from a CO_2 laser which is out of phase with the temperature fluctuations associated with the hydrothermal waves at the location of the sheet. Nahas & Panton (1990) have used a similar technique to drive opposing flows on the surface of a jet undergoing acoustically forced capillary breakup, thus delaying the formation of droplets. Recently, Petrov *et al.* (1996) have employed a nonlinear control algorithm using temperature measurements near the free surface and heating with a thermoelectric element to suppress oscillations of thermocapillary convection in liquid bridges.

2. Experimental setup and procedure

The apparatus employed for these experiments is the same as used in the experiments reported in Part 1; figure 1 of that paper provides a sketch of the geometry of the layer. To demonstrate the feasibility of control, we concentrate on the suppression of hydrothermal waves for a layer $d = 1$ mm in depth, corresponding to axial (L/d) and transverse (W/d) aspect ratios of 30 and 50, respectively, and a dynamic Bond number of $Bo_D = 0.142$.

The output of the CO_2 laser is focused and formed into a sheet which is used to heat a line of small thickness on the free surface of the liquid layer downstream (with respect to the wave-propagation direction) of the thermocouple locations at which input data characterizing each hydrothermal wave are collected. The plan is to selectively heat the troughs of disturbance temperature, thereby locally raising the temperature there and hopefully disrupting the instability mechanism described by Smith (1986).

The control of a particular hydrothermal wave is achieved using data measured specifically for that wave, necessitating the use of a delay in the *feed-forward control* scheme to be described. The signal from the infrared camera described in Part 1 is first converted into a video signal, which is output to a video-cassette recorder (VCR) for recording and to a frame grabber for real-time analysis. The images from the frame grabber are processed in the following fashion, illustrated in figure 1, to

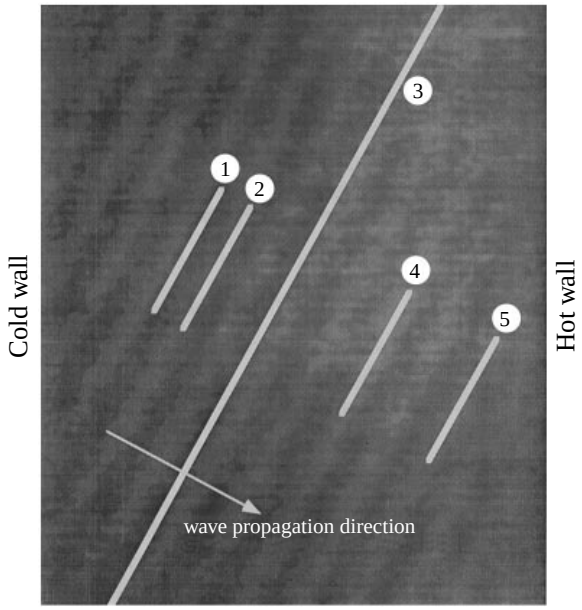

FIGURE 1. Overhead view of layer, showing hydrothermal waves and locations of data (1, 2, 4 and 5) and heating (3) lines.

initiate the control. Two lines (identified by the numerals 1 and 2 in figure 1) which are parallel to the observed hydrothermal-wave crests and located upstream of the known control site (line 3 in figure 1) are selected as input data locations. Along these lines, each of which occupies 79 pixels, the luminance data are averaged to smooth the noise resulting from pixel-to-pixel variations. The 79-pixel line length is the longest line which can be used and still perform the control in real time, given the limitations of the computer employed. The time histories of these averaged signals are used to compute the phase speed of each hydrothermal wave which passes. The distance between lines 1 and 2 is less than the wavelength of a hydrothermal wave so there is no ambiguity in the determination of this phase speed. As mentioned above, downstream of lines 1 and 2 is a line identified by 3 placed at the location where the laser heating is to be delivered.

The *output signal* to the laser controller is created in the following fashion. The line-averaged luminance signal from line 2, called the *raw input signal*, is jump-limited and drift compensated using a running time mean. A constant input gain and a constant offset (which are set manually at the beginning of every experiment) are applied to this signal to shift it into a window (with a value range $[-1, 1]$) that is suitable for further processing and monitoring on an oscilloscope. This processed input signal is then temporarily stored in a buffer, so that the output signal may be delayed to allow for the hydrothermal-wave transit time between lines 2 and 3. Data read from the buffer at a location corresponding to the proper time delay are then inverted, gain adjusted and offset to construct an output signal within the 0–10 V range required by the laser controller. This output signal, tailored to each passing hydrothermal wave, allows the delivery of laser heating to each hydrothermal-wave temperature trough to suppress the oscillations. Lines 4 and 5 in figure 1 are used for the collection of data used to assess the effectiveness. Output gain and offset

may be varied manually during experiments in order to investigate the effect of the magnitude of laser power on the control.

A previous attempt at control was made by Riley (1995) using a fine-wire thermocouple placed near the corner of the flow field from which the hydrothermal waves appear to emanate. The signal coming from the thermocouple was inverted, gain adjusted, phase shifted and sent to the laser controller, as above, but the phase shift of the signal had to be adjusted manually due to a lack of knowledge of the phase speed of the waves. The initiation of control was found to be extremely sensitive to this choice of phase shift. When wave suppression was achieved, it was not possible for it to be maintained for more than roughly a half dozen cycles, due to a combination of factors. First, the advection of a portion of the laser energy to the thermocouple location through the vigorous free-surface motion of the basic state causes a change in the signal there. Secondly, slight modification of the wave pattern upstream of the control location is observed following the successful initiation of suppression which necessitates a further change in phase shift of the laser input. The manual setting of this phase shift, coupled with the sensitivity of the system to its choice, did not permit this adjustment to be made, as it is automatically with the present scheme. Therefore, although this intrusive scheme was able to demonstrate that wave suppression is possible for at least a few cycles, data from a single-point measurement are not sufficient to permit tailoring the control scheme to specific waves, as described above.

In implementing the present control scheme described above, there are a couple of points to keep in mind. First, as mentioned in the previous paragraph, the free-surface flow is in a direction opposite to that of the streamwise component of the phase velocity of the hydrothermal waves and is large compared with the phase speed. For instance, for the case considered in this paper, the free-surface speed of roughly 7 cm s^{-1} is relatively large compared with the hydrothermal-wave phase speed of approximately 2 mm s^{-1}. Hence, for the 1 cS silicone oil ($Pr = 13.9$) used in these experiments, large temperature changes created by the laser heating can be advected to the read lines (1 and 2 in figure 1), potentially degrading the quality of the input signal necessary to accomplish the suppression. Second, the hydrothermal waves which appear following the onset of instability are large everywhere in the flow domain (see also figures 8 and 9 of Part 1). On the other hand, the T–S waves of interest in the Liepmann & Nosenchuck (1982) experiment are convective in nature, growing in the flow direction. The hydrothermal-wave instability thus appears somewhat reminiscent of an absolute instability in character, which may have further negative implications from the standpoint of suppression, particularly if the absence of oscillatory flow is required everywhere in the layer.

Figure 2 shows an overall schematic of the control experiment. The laser employed for these experiments is a Synrad (48-1-115W) CO_2 laser, with variable output power ranging from 0 to 10 W at 10.6 μm, which is controllable with an analog input voltage between 0 and 10 V. The laser beam has a nominal diameter of 3.5 mm, but is allowed to expand in this experiment for slightly less than 2 m to assure the existence of a Gaussian beam. Once expanded, the beam (now 7 mm in diameter) passes through a 3 mm diameter aperture and is directed toward the flow apparatus by an angled mirror. It then passes through a zinc-selenide lens with a 250 mm focal length before being reflected by a concave cylindrical mirror with a focal length of −12.7 mm. This mirror serves to redirect the beam downward toward the free surface of the liquid and simultaneously expand it into a sheet. This sheet of 10.6 μm infrared radiation intersects the free surface of the liquid, producing the desired line-heating source for the control output.

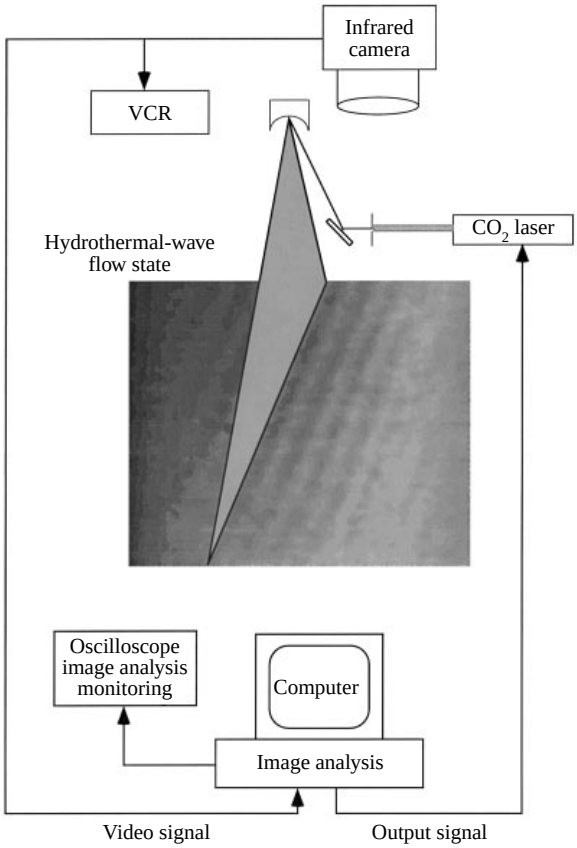

FIGURE 2. Schematic of the control experiments.

For the control scheme to be successful, the thickness of the infrared sheet can be no greater than one-half of the wavelength of the hydrothermal waves. Since a 1.0 mm deep layer is investigated in these control experiments, and the experimentally determined critical wavelength for that depth is $\lambda = 2.58$ mm (table 2, Part 1), a sheet thickness of about 1 mm is desired. In order to measure this thickness, a piece of Plexiglas is heated and observed using the infrared camera. A graph of the line luminance normal to the heated line is shown in figure 3. From this profile, the estimated full-width-at-half-maximum sheet thickness is 1.14 mm, which is less than one-half of the disturbance wavelength for the layer examined in these experiments. This measurement technique should yield a relatively good estimate for the laser-sheet thickness. In the limit of zero thermal conductivity, the image of the heated area yields the true sheet thickness since the heat does not diffuse away from the line of application. Since Plexiglas has a relatively low thermal conductivity, the thickness determined in this fashion is only slightly greater than the true sheet thickness of the infrared sheet.

Since the CO_2 beam is invisible, the alignment of the optical system is a non-trivial undertaking. Optical alignment is accomplished by placing strips of Plexiglas in the optical path, and burning them with the beam. This allows the alignment of each optical component with the burned spot. Once the beam is finally expanded into a sheet, a rough alignment with the flow apparatus is performed using thermally

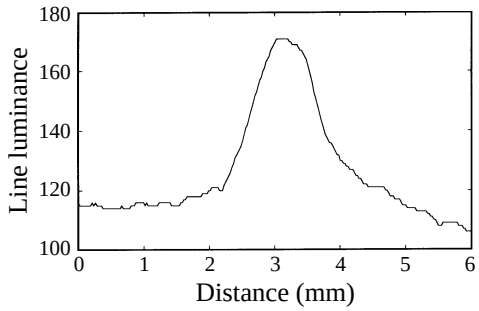

FIGURE 3. Line-luminance trace across a heated line on a Plexiglas surface.

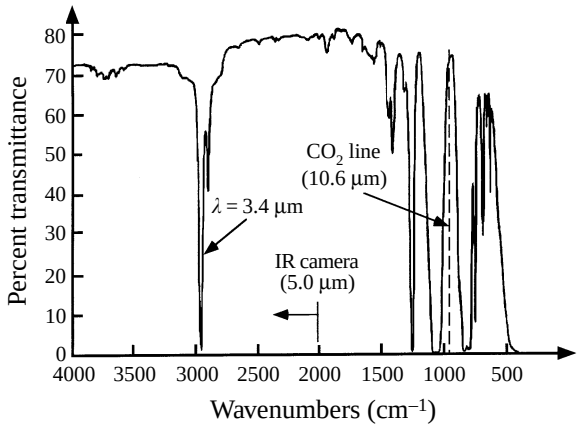

FIGURE 4. Absorption spectrum from a smear sample of 1 cS silicone oil.

sensitive beam-probe plates in conjunction with an ultraviolet light source. Final alignment of the sheet with respect to the obliquely propagating hydrothermal waves is accomplished using the infrared camera described in Part 1 to locate the position and orientation of the heated line with the hydrothermal-wave pattern present in the flow apparatus. Since either of two possible wave families may appear (Smith & Davis 1983), a mechanism allows the concave mirror to be rotated to always allow heating parallel to the wave crests of the observed family.

A final note on the experimental setup and data collection concerns the absorption properties of 1 cS Dow Corning 200 silicone oil. Figure 4 shows an absorption spectrum of a smear sample of 1 cS silicone oil measured by colleagues in the Georgia Institute of Technology School of Chemistry and Biochemistry. Two absorption bands of importance are marked in the figure. The band at 3.4 μm is what is 'seen' by the infrared camera, and the line at 10.6 μm denotes the wavelength of the CO_2 laser corresponding to the heating. The camera is virtually insensitive to anything to the right of the line marked at 5.0 μm. This is important, because it allows the camera to detect the thermal field in the liquid, without being blinded by the much stronger laser emission at 10.6 μm. However, the fact that a heated line on the surface of the fluid layer appears as a dark stripe (see figure 5*d*) indicates that some of the reflected radiation at 10.6 μm is picked up by the IR-camera. Also note that the absorption at 10.6 μm is relatively weak, but since this spectrum is collected for a smear sample the implication of this is uncertain. The data of Pline (1989) for 10 cS silicone oil display

a very similar spectrum to that measured for the 1 cS oil, and absorption results for a 100 μm-thick liquid sample indicate nearly total absorption. If one assumes similar results to hold for the 1 cS oil used in the present experiments, one would conclude that the heating of the liquid at the free surface actually occurs in a thin layer at the free surface of roughly 100 μm thickness. For a total layer depth of 1 mm, this would imply that the 'surface' heating in these experiments occurs within the top 10% of the liquid layer. We shall see in §3, however, that subsequent measurements indicate that this may not be the case.

3. Results and discussion

The control scheme described above was applied to suppress hydrothermal waves for a 1 mm deep layer at a laboratory Marangoni number of approximately $Ma_L \approx 575$. The critical Marangoni number corresponding to this layer depth presented in Part 1 is $Ma_L = 440$, so that this layer is substantially supercritical. In addition to the technique just described of pulsing the laser using the signal from the upstream waves, the influence of a constant laser power is also investigated. The effectiveness of the control is assessed by examining line-averaged pixel luminance data in thermographic images which correspond to free-surface temperature fluctuations at locations both upstream and downstream of the control site. For all thermographs presented in this paper, the cold and hot walls of the apparatus are at the left- and right-hand sides, respectively, and the hydrothermal waves propagate from upper-left to lower-right.

3.1. *Time-dependent heating*

This technique is the one described in §2 above, whereby the time-dependent laser power delivered to the IR sheet is adjusted based on the signals from the data read lines (lines 1 and 2 in Figure 1). The magnitude of the laser power delivered to the fluid layer is controlled by manually setting the values for output-signal gain and offset. By properly setting these two parameters it is assured that the output-signal troughs are very close to zero, meaning that virtually no heat is delivered to the high-surface-temperature locations of the hydrothermal waves. Also, by adjusting output gain and offset in such a fashion, the relative differences between the peak-to-peak and the zero-to-peak amplitudes of the output signal can be reduced to less than 10%.

Figure 5 shows four instantaneous thermographs of the layer free surface taken while operating in this mode. The image in figure 5(*a*) is of the layer prior to initiating control, showing pure hydrothermal waves. Dark regions correspond to cold spots, while light regions indicate high surface temperature. In figure 5(*b*), control is attempted with the laser set at an intermediate power level. Some attenuation of waves is visible downstream from the heating location with hydrothermal wave suppression being stronger in the vicinity of the hot wall. As depicted in figure 5(*c*) this tendency is enhanced as the laser power is increased. Finally, for the power level used in figure 5(*d*), the thermograph is shown at an instant when the laser power is near its maximum so that the location of the heating line is also clearly visible.

From a visual inspection of these thermographs, it is clear that the application of the technique has resulted in the disappearance of hydrothermal waves downstream of the heating location. Figure 6, however, shows evidence of the effectiveness of the control of a more quantitative nature. In figure 6(*a*), the time histories of the line-averaged luminance from lines 2 and 4 are plotted for a case prior to the initiation of control; in figure 6(*b*) the same quantities are shown after the start of periodic heating at a power

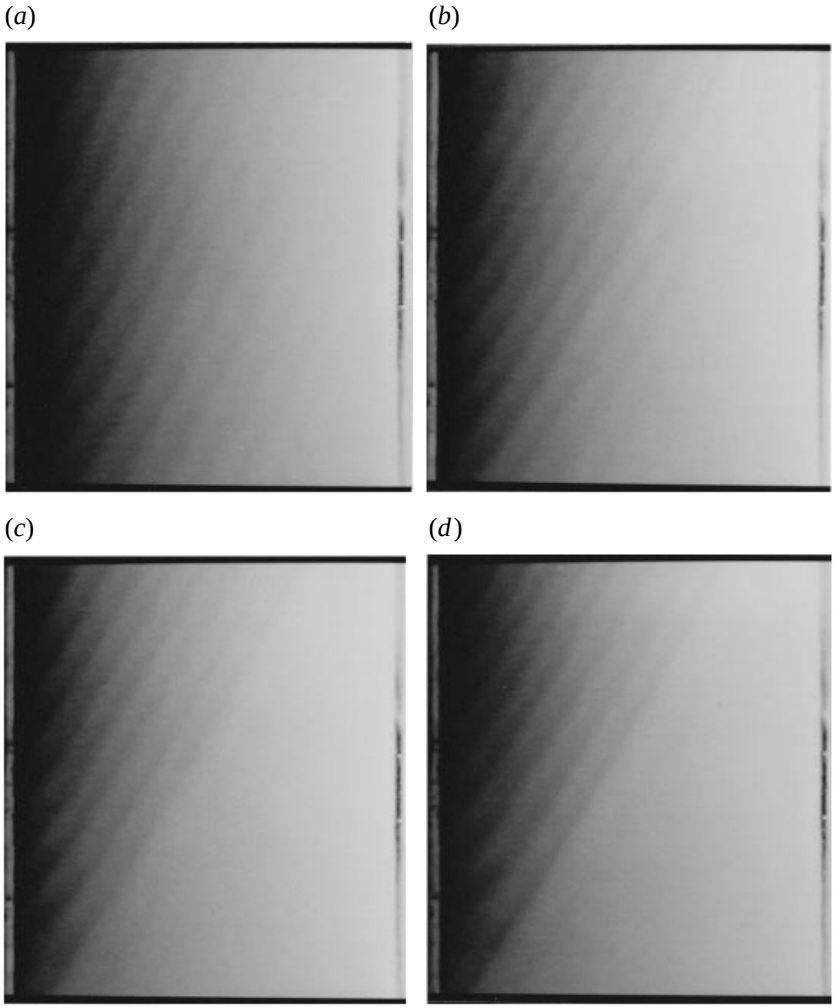

FIGURE 5. Infrared thermographs showing effectiveness of the time-dependent control scheme at various laser-aperture power (zero-to-peak) levels: (*a*) 0 W; (*b*) 1.3 W; (*c*) 2.2 W; (*d*) 3.3 W.

level which corresponds to the state shown in figure 5(*d*). It may be observed that the line 2 data are slightly affected (a small amplitude increase may be observed) by the application of periodic heating, while the peak-to-peak amplitude of the signal at line 4 has been reduced through control from a line-averaged luminescence of roughly 5 to one of $O(0.5)$, which is within the data noise level (determined from Fourier spectra to be discussed in the next paragraph). Control is achieved within roughly 30–45 s of turning on the laser and may be maintained virtually indefinitely. As noted in §2, earlier experiments performed using a single-point intrusive thermocouple (Riley 1995) to initiate the laser were only successful in obtaining a few cycles of control, due to a combination of a lack of knowledge of the hydrothermal-wave phase speed and to feedback from the heating line to the thermocouple.

The influence of laser power level on control was investigated using an experimental protocol which manually stepped the laser power from zero in variable increments of $O(0.5$ V) peak-to-peak, holding the laser power at each level for roughly 3 minutes.

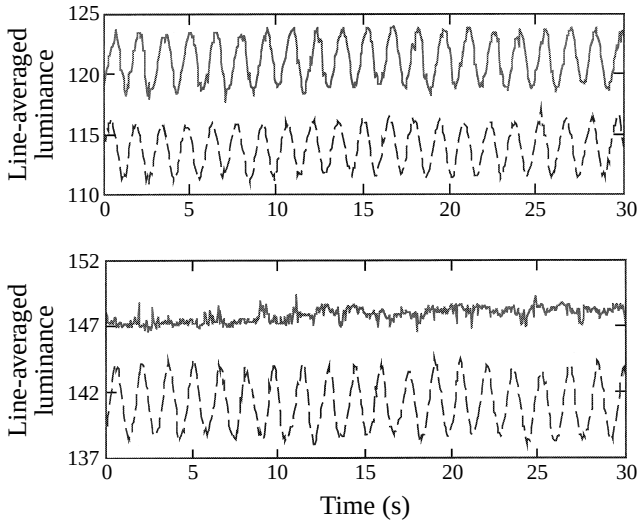

FIGURE 6. Line-averaged luminance from upstream (line 2–dashed) and downstream (line 4–solid) data-read lines for the time-dependent control scheme: (*a*) no control (data from line 4 have been offset by a luminance value of 38 to allow both curves to be displayed together); (*b*) laser-aperture power (zero-to-peak) of 3.3 W, corresponding to the thermograph seen in figure 5(*d*) (data from line 4 have been offset by a luminance value of 45 to allow both curves to be displayed together).

This is more than enough time for the flow to accommodate to the new power, as verified from examining the Fourier spectra computed at different time intervals within the 3-minute window (the transition time seen in the Fourier analysis is around 30 to 45 s). The following results are based on the amplitudes of the primary Fourier modes, taken during the last 37 s of these windows. Line-averaged luminance data are gathered at a rate of 15 Hz at each of lines 1, 2, 4 and 5 of figure 1. To determine the dominant component, thirty-one Fourier transforms are computed on a sliding data set of 256 consecutive data points. Since a discrete Fourier transform is employed, the observed oscillations do not consist of a pure mode, i.e. with all power in a single Fourier component. Rather, the vast majority of the power is always contained in two adjacent modes which correspond to frequencies of 0.59 and 0.64 Hz. The mean value of these two Fourier components is nearly constant during the 37 s period at the end of the 3-minute data window. Therefore, the analysed data correspond to a state, which, after the previous increase of laser power, has relaxed to a new equilibrium. The mean of these two largest Fourier amplitudes, is further time-averaged over the 37 s data-analysis window and reported as the 'Fourier amplitude' in what follows. Figure 7(*a*) shows the variation of this Fourier amplitude as a function of zero-to-peak voltage delivered to the laser at each of lines 1, 2, 4 and 5 for a single experiment. Lines marked as (i)–(iv) on this figure correspond to the power levels employed in the experiments which produced the thermographs in figure 5(*a*)–(*d*), respectively. At a power level slightly below 1 V, the amplitude at the downstream lines (4 and 5) begins to decrease, indicative of the effectiveness of the heating in suppressing the hydrothermal waves.

Also observed in figure 7(*a*) is an upward drift in Fourier amplitude at the upstream lines (1 and 2). This was mentioned in the discussion of the line 2 data from figure 6. While the precise cause for this behaviour is not known for certain, some reasons may be speculated. The heating at line 3 is observed to raise the mean temperature

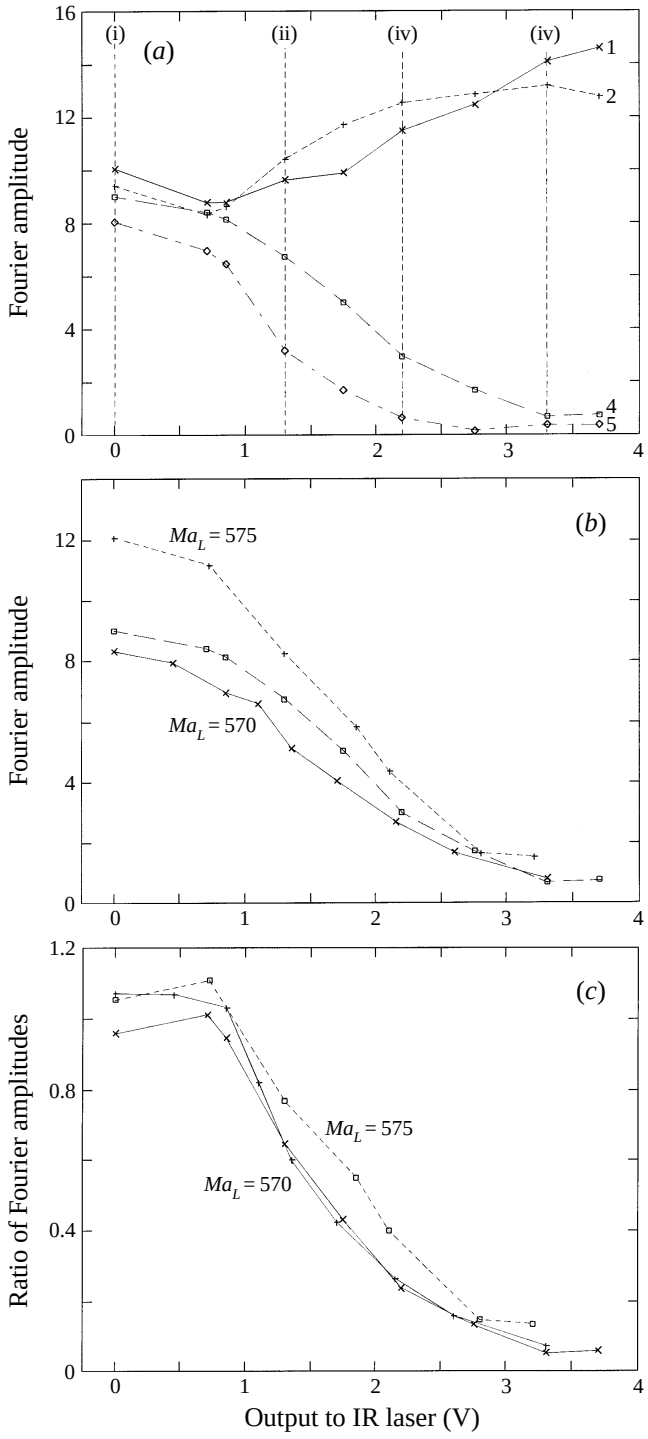

FIGURE 7. Spectral evaluation of the influence of laser power for the time-dependent control scheme: (*a*) single experiment, showing the behaviour at the four data-read lines (vertical lines show the power levels corresponding to those of figure 5); (*b*) line 4 data from three different sets of experiments; (*c*) line 4 data from three different sets of experiments normalized by the corresponding line 2 data upstream of the heating location.

of the fluid at locations 1 and 2, but this has no direct effect on the values plotted in figure 7(*a*) because only the pair of dominant modes of the oscillatory component are being shown there (only the Fourier components corresponding to 0.59 Hz and 0.64 Hz are considered, as discussed above). A possible indirect effect, however, may be important since the increase of mean temperature at lines 1 and 2 results in a slight increase of the time-averaged local temperature gradients upstream from the heating line (recall that lines 1 and 2 are near the cold wall of the apparatus). Therefore, the local Marangoni number Ma discussed in Part 1 is increased as laser power increases, and this fact could possibly explain the increases observed in the line 1 and 2 values. During the experiments which produced the hydrothermal waves reported here (i.e. in the range $450 < Ma_L < 570$), it is found that the amplitude of hydrothermal waves does increase with increasing Marangoni number. A systematic investigation to determine the amplitude of these free-surface temperature fluctuations and their dependence on experimental parameters has not been performed, hence the above discussion remains speculative.

In figure 7(*b*), results of line 4 data are shown for three different sets of experiments, indicating the reproducibility of the influence of laser power level. From these curves, one might mistakenly conclude that the amplitude of the surface-temperature fluctuations at $Ma_L = 575$ is somewhat larger than at $Ma_L = 570$. However, this conclusion cannot be drawn. The values plotted in figure 7(*b*) are a quantitative measure of the luminance variations in the analysed infrared images which depend linearly on the surface-temperature variations. The linear dependence is determined by the infrared image gain and offset, two parameters that are set manually in the infrared camera controller and were varied from experiment to experiment. The somewhat larger values plotted in figure 7(*b*) at $Ma_L = 575$ result from using a larger infrared image gain in that particular experiment. The increase of hydrothermal-wave amplitude with Marangoni number which was mentioned earlier therefore does not emerge from figure 7(*b*). Perhaps the most instructive and independent of assessment parameters is the relative attenuation of the hydrothermal waves shown in figure 7(*c*), where the line 4 data are scaled by the respective amplitudes at line 2 for each laser power.

It is clear that the degree of amplitude reduction is directly correlated with power supplied to the laser. Further, at a power level of about 2.5–3 V, the luminance oscillation amplitudes have disappeared into the noise level, indicating that maximum possible control has been achieved.

3.2. *Constant heating*

For this set of experimental trials, the positions of all lines in figure 1 were left unchanged from those of the time-dependent-heating case. The difference is that, for these experiments, the heating provided by the laser is constant in time, manually set to different values to again assess the influence of laser power. Therefore, the entire active-control algorithm described above is bypassed. Lines 1, 2, 4 and 5, however, are still used to record data for the purposes of evaluation.

Figure 8 shows the behaviour of the dominant oscillatory Fourier component of the line-averaged luminance at lines 1, 2, 4 and 5 as a function of laser power for a single experiment. For low-to-moderate values of laser power the behaviour of these modes is reminiscent of what is observed in the time-dependent cases: for low enough values of the laser power, control is absent; as power increases, attenuation of the Fourier mode is seen at the locations downstream of the heating line. What is different in these experiments, however, is the fact that signal attenuation is also

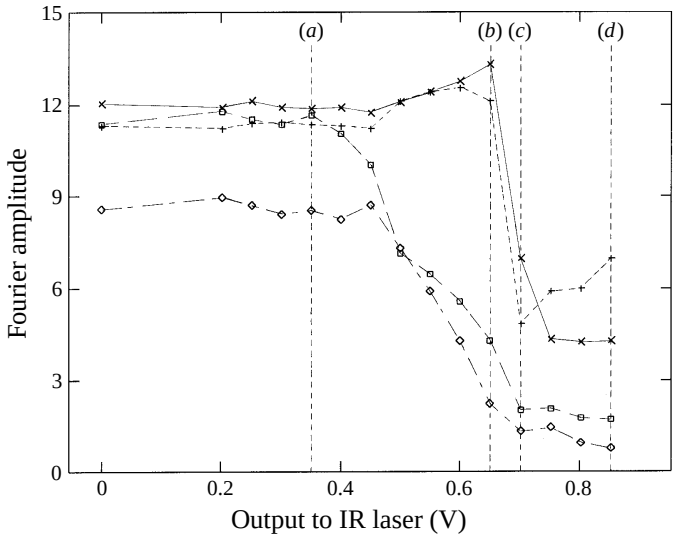

FIGURE 8. Spectral evaluation of the influence of laser power for the constant-heating control scheme for a single experiment, showing the behaviour at the four data-read lines (vertical lines show the power levels corresponding to those of figure 9).

observed upstream (lines 1 and 2) of the heating line for large enough values of laser power, suggesting that the influence of the constant heating may be to suppress waves everywhere in the layer. This, however, is not actually the case, as the following discussion shows.

Figure 9 shows a sequence of four thermographs of the layer corresponding to different magnitudes of constant laser heating; the four corresponding power levels are indicated on figure 8 by the letters (*a*), (*b*), (*c*) and (*d*) respectively. At the lowest of the continuous-power levels seen in figure 9(*a*), the heating at line 3 has no visible effect on the hydrothermal waves. Figure 9(*b*) shows a thermograph taken at a somewhat higher laser power level at which some suppression of wave behaviour in the vicinity of the heating line can be noticed. This is contrary to what is observed at lower power levels in the time-dependent case, where suppression is observed closer to the hot wall, moving toward the heating line as power is increased. Note that the steady output voltages employed in the constant-heating experiments are much smaller (by a factor of 5; see figures 7 and 8) than those (zero-to-peak) used in the time-dependent control scheme. As laser power is increased to the value corresponding to the thermograph in figure 9(*c*), the wave structure at locations upstream of the line has lost some of the regularity observed for lower power levels and a clear change in the propagation angle of the upstream waves is evident. Finally, the thermograph of figure 9(*d*) corresponds to a power level for which the spectral results in figure 8 indicate a strong attenuation of waves downstream from the heating location but also a greatly reduced amplitude upstream. However, upstream of the heating line a well-defined group of waves is visible in the thermograph, but at a different angle than those observed for lower heating. The misalignment of these wave crests with read lines 1 and 2 now means that the line averages along these lines will cross wave crests, yielding a smaller fluctuating value, reflected in the reduced magnitude of the Fourier component.

As discussed above for the case of time-dependent heating, the application of steady

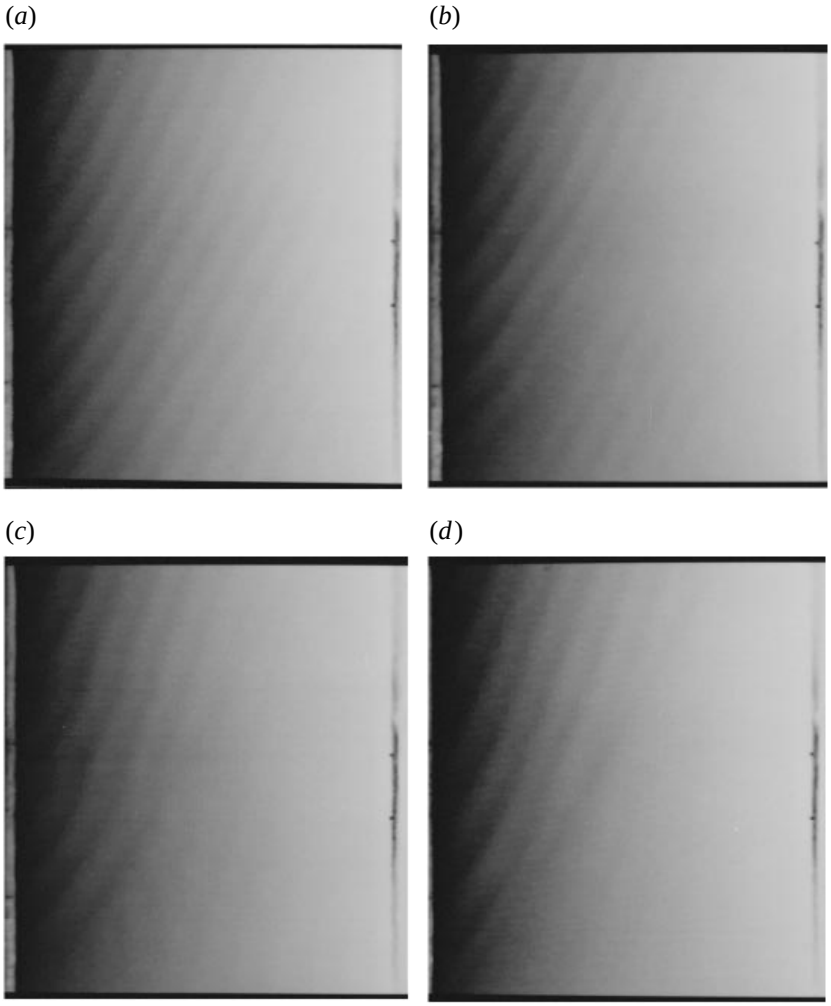

FIGURE 9. Infrared thermographs showing effectiveness of the constant-heating control scheme at various laser-aperture power (zero-to-peak) levels: (*a*) 0.35 W; (*b*) 0.65 W; (*c*) 0.7 W; (*d*) 0.85 W.

heating undoubtedly affects the structure of the basic state itself. In particular, the mean-temperature gradient between line 3 and the hot wall is reduced by the heating; consequently, the local Marangoni number *Ma* in this region is reduced. As *Ma* is reduced, the amplitude of hydrothermal waves will decrease; if *Ma* falls below the critical value for the onset of hydrothermal waves, then waves should not appear there, and this is the likely reason for their observed disappearance. Therefore, it appears that steady power levels supplied to the layer in this manner have changed the underlying structure of the basic state, and hence, the instability. This is not the case with time-dependent heating. Evidence of this is provided by the earlier experiments performed using a thermocouple as the source of the input signal. As mentioned in §2 and §3.1, these experiments were extremely sensitive to the manually chosen phase shift: if this was not selected properly, hydrothermal waves covered the entire free surface, both upstream and downstream of the heating, in spite of the fact that heating was being applied. Also, following the loss of control in those

experiments, waves reappeared at both upstream and downstream locations. If the periodic heating were affecting the layer in the same manner as in the constant-heating experiments, one would expect the downstream waves to be absent, which was not the case. Consequently, the application of steady heating parallel to the crests of the originally appearing hydrothermal waves is perhaps a less attractive way to achieve control than the time-dependent scheme described in §3.1.

3.3. *Energy transmission estimate*

In addition to obtaining these results, an energy balance was performed to estimate the effect of the incident radiation. From the results of Pline (1989) for 10 cS silicone oil, it was estimated the majority of the absorbed energy at the 10.6 μm emission line is absorbed in a layer of roughly 100 μm thickness. Thus, the volume of fluid which absorbs radiation from the CO_2 laser is equal to the surface area which is exposed multiplied by the 100 μm thickness of the absorption layer. The time during which the heating is active is that time necessary for the local temperature depression to pass the heating line, which, for the case of a 1.0 mm-deep layer at the critical Marangoni number, is approximately $\Delta t = 0.8$ s. An approximate energy balance yields

$$\rho c_p V \Delta T = \overline{Q}_{abs} \Delta t - \dot{m} c_p (\overline{T}_{out} - \overline{T}_{in}),$$

where the term on the left-hand side represents the temperature rise of the liquid volume under the applied radiative flux, the first term on the right-hand side is the radiative energy absorbed by the layer, and the last term is the energy convected out of the control volume. Conductive and radiative losses from the layer have been neglected as they are small, and any additional convection induced by the radiative heating has also been neglected. In the equation above, ρ is the density, c_p the specific heat, V the fixed volume beneath the applied heating (50 mm × 1.2 mm × 0.1 mm), $\overline{Q}_{abs}$ is the average absorbed radiative power, $\dot{m}$ the mass flux through the control volume due to the basic state velocity profile, and $(\overline{T}_{out} - \overline{T}_{in})$, the average temperature rise of the fluid convected through the control volume. Using this result, one may calculate that, to effect a temperature change of $\Delta T = 0.5$ °C (the peak-to-peak variation observed at $Ma_L = 575$), the required peak radiative power, Q_{peak}, absorbed by the liquid layer should be about 25 mW. This is an extremely small value; in fact, it is two orders of magnitude below the applied aperture laser-power level of roughly 3 W employed in the control experiments.

To further investigate this apparent discrepancy, an energy-balance experiment was performed for a 1 cS silicone-oil layer under the same conditions experienced by the liquid in the flow apparatus. An insulated liquid layer of volume $V = 10$ cm^3 was placed at the location normally occupied by the flow apparatus and exposed to the CO_2 laser sheet at a power level comparable to that employed for the control experiments ($P \approx 2.5$ W @ the laser aperture) for a period of 5 minutes. The change in the mean temperature of the layer following this exposure was $\Delta T \approx 0.9$ °C. Accounting for the optical losses in the experimental setup, it was estimated that the amount of energy reaching the free surface of the liquid is roughly 15% of the 2.5 W output by the laser. Therefore, of the roughly 110 J of energy incident upon the liquid layer, only 12.5 J were actually absorbed, indicating an absorption efficiency of 11%. Using the calculated absorption efficiency of 11%, the aperture laser power required to deliver the estimated peak absorbed radiative power of $Q_{peak} \approx 25$ mW is approximately $P_l \approx 1.5$ W, which compares reasonably well with the observed values of $P_l \approx 3.0$ W used in the control experiments.

It is interesting to note that the measured absorption efficiency of 11% for the 1 cS

silicone oil is in contrast to the assumption made on the basis of results for 10 cS silicone oil, which Pline (1989) determined to be totally absorbing at a layer depth of 100 μm. Therefore, the smear sample of the 1 cS silicone oil shown in figure 4 probably provides a correct picture when it indicates that the 1 cS silicone oil used in these experiments is not very absorptive at the 10.6 μm spectral line corresponding to the laser output.

From the experimental results, one observes that excellent control of the hydrothermal waves is achieved with an output voltage to the laser of 3 V zero-to-peak (see, e.g. figure 7*c*). Using the efficiency calculated above, the power absorbed in the fluid layer for this output voltage is roughly 50 mW. This flux is approximately ten times that calculated as necessary to erase the hydrothermal-wave free-surface temperature depression.

4. Conclusions

The experiments described above have demonstrated the feasibility of suppressing oscillatory thermocapillary convection in thin liquid layers subject to a horizontal temperature gradient. Based upon the instability mechanism suggested by Smith (1986), control was achieved by heating troughs of low disturbance temperature with a sheet of IR radiation. The active feed-forward control scheme employed in these experiments is conceptually simple but effective for the suppression of hydrothermal waves in a high-Prandtl-number liquid.

Two features of the described experiments were key to their success: (i) the non-intrusive sensing of the surface-temperature fluctuations using an infrared camera; and (ii) the real-time determination of the hydrothermal-wave phase speed, allowing the control input to be precisely tailored to each hydrothermal wave. Earlier attempts at control by Riley (1995) using a thermocouple inserted below the free surface of the liquid achieved limited success due to the reliance on a single-point measurement and, perhaps, to the intrusive nature of the thermocouple inserted through the liquid free surface. The manual adjustment of the phase and amplitude of the forcing in those experiments made it impossible to suppress the oscillations for more than a few cycles.

There remain questions regarding the effectiveness of the CO_2 laser in providing surface heating to the 1 cS silicone oil employed for these experiments. Clearly, the laser is sufficiently powerful to accomplish the task, but the precise depth range of the applied heating is still unknown, as is the importance of this range. The work of Smith (1986) implies that, for high-Prandtl-number liquids, surface-temperature disturbances are coupled, through a convective process, to thermal disturbances in the bulk to sustain the instability. Hence, heating supplied to the bulk as well as to the surface may also provide a means of breaking this coupling.

Finally, the eventual use of such a technique in suppressing oscillations occurring during the float-zone crystal-growth process requires additional thought. First, such crystal-growth situations involve liquid metals of extremely small ($O(10^{-2})$) Prandtl number, so that the mechanism of the instability is different, as observed by Smith (1986) for planar layers and later by Levenstam & Amberg (1995) for a cylindrical geometry. In the planar case, hydrothermal waves propagate transversely across the layer, normal to the mean temperature gradient, meaning that the elimination of oscillations at the cold wall (solidification front) would require the simultaneous suppression of waves in the entire layer. For a cylindrical geometry exhibiting relatively few waves propagating in the azimuthal direction, this may or may not be possible.

We wish to thank Professor D. F. Jankowski for originally suggesting the idea of suppressing hydrothermal waves, Professor M. K. Smith for helpful discussions regarding the instability mechanism, Professor M. Yoda for assistance with the sheet-formation optics and colleagues in the School of Chemistry and Biochemistry at the Georgia Institute of Technology for performing the smear-sample spectrum shown in figure 4. Finally, we express our deep appreciation to Professor D. Schwabe for allowing Messrs. Benz and Hintz to each spend six months in Atlanta working on this project. This work was supported by the Microgravity Research Division, Office of Life and Microgravity Science and Applications of NASA. Additional travel funds were provided by DARA under contract number 50 WM 9446.

REFERENCES

Gatos, H. C. 1982 Semiconductor crystal growth and segregation problems on earth and in space. In *Materials Processing in the Reduced Gravity Environment of Space* (ed. G. E. Rindone). Elsevier.

Levenstam, M. & Amberg, G. 1995 Hydrodynamical instabilities of thermocapillary flow in a half-zone. *J. Fluid Mech.* **297**, 357.

Liepmann, H. W., Brown, G. L. & Nosenchuck, D. M. 1982 Control of laminar-instability waves using a new technique. *J. Fluid Mech.* **118**, 187.

Liepmann, H. W. & Nosenchuck, D. M. 1982 Active control of laminar-turbulent transition. *J. Fluid Mech.* **118**, 201.

Nahas, N. M. & Panton, R. L. 1990 Control of surface tension flows: instability of a liquid jet. *Trans ASME*: *J. Fluids Engng*. **112**, 296.

Neitzel, G. P., Law, C. C., Jankowski, D. F. & Mittelmann, H. D. 1991 Energy stability of thermocapillary convection in a model of the float-zone crystal-growth process. II: Nonaxisymmetric disturbances. *Phys. Fluids* A **3**, 2841.

Petrov, V., Schatz, M. F., Muehlner, K. A., VanHook, S. J., McCormick, W. D., Swift, J. B. & Swinney, H. L. 1996 Nonlinear control of remote unstable states in a liquid bridge convection. *Phys. Rev. Lett*. **77**, 3779.

Pline, A. D. 1989 Infrared surface temperature measurements for the surface tension driven convection experiment. *NASA* TM-101353. NASA Lewis Research Center.

Riley, R. J. 1995 An investigation of the stability and control of a combined thermocapillary-buoyancy driven flow. PhD Thesis, Georgia Institute of Technology.

Riley, R. J. & Neitzel, G. P. 1998 Instability of thermocapillary–buoyancy convection in shallow layers. Part 1. Characterization of steady and oscillatory instabilities. *J. Fluid Mech.* **359**, 143–164.

Shen, Y., Neitzel, G. P., Jankowski, D. F. & Mittelmann, H. D. 1990 Energy stability of thermocapillary convection in a model of the float-zone crystal-growth process. *J. Fluid Mech.* **217**, 639.

Smith, M. K. 1986 Instability mechanisms in dynamic thermocapillary liquid layers. *Phys. Fluids* **29**, 3182.

Smith, M. K. & Davis, S. H. 1983 Instabilities of dynamic thermocapillary liquid layers. Part 1. Convective instabilities. *J. Fluid Mech.* **132**, 119.

Tang, J. & Bau, H. H. 1993 Stabilization of the no-motion state in Rayleigh-Bënard convection through the use of feedback control. *Phys. Rev. Lett*. **70**, 1795.

Wanschura, M., Shevtsova, S., Kuhlmann, H. C. & Rath, H. J. 1995 Convective instability mechanisms in thermocapillary liquid bridges. *Phys. Fluids* **7**, 912.